第 26 卷第 5 期
2010 年 5 月

无 机 化 学 学 报
CHINESE JOURNAL OF INORGANIC CHEMISTRY

Vol.26 No.5
832-838

Mn_2O_3 纳米结构的简易合成与电化学性质

赵 丹[1,2] 谭金山[1] 季倩倩[1,2] 张进涛[3] 赵修松[1,2,3] 郭培志*[,1,2]

([1]青岛大学纤维新材料与现代纺织国家重点实验室培育基地多功能材料研究所,青岛 266071)

([2]青岛大学化学化工与环境学院,青岛 266071)

([3]Department of Chemical and Biomolecular Engineering, National University of Singapore, 4 Engineering Drive 4, Singapore 117576)

摘要: 用简易的室温或水热方法制备出不同形貌的 $MnCO_3$ 微结构。经 600 ℃热处理后,室温制备 $MnCO_3$ 转变成 Mn_2O_3 胶体片,而水热制备 $MnCO_3$ 样品则形成多孔 Mn_2O_3 纳米结构。然而,室温制备 $MnCO_3$ 经 120 ℃热处理后形成 Mn_2O_3 晶相。制备样品经过 XRD 和 SEM 表征表明,热处理 $MnCO_3$ 前驱物形成 Mn_2O_3 过程导致产物形貌与结构变化。其形成机理又通过 TEM 和 FTIR 进一步研究。Mn_2O_3 纳米结构的电容性质通过循环伏安法表征,结果表明 Mn_2O_3 形貌与结构对其电容有重要影响。

关键词: Mn_2O_3; $MnCO_3$; 水热合成; 电容

中图分类号: O614.7; O611.62 **文献标识码**: A **文章编号**: 1001-4861(2010)05-0832-07

Mn_2O_3 Nanomaterials: Facile Synthesis and Electrochemical Properties

ZHAO Dan[1,2] TAN Jin-Shan[1] JI Qian-Qian[1,2] ZHANG Jin-Tao[3]

ZHAO Xiu-Song[1,2,3] GUO Pei-Zhi*[,1,2]

([1]*Institute of Multifunctional Materials(IMM), Laboratory of New Fiber Materials and Modern Textile, The Growing Base for State Key Laboratory, Qingdao University, Qingdao, Shandong* 266071)

([2]*College of Chemistry, Chemical Engineering and Environment, Qingdao University, Qingdao, Shandong* 266071)

([3]*Department of Chemical and Biomolecular Engineering, National University of Singapore, 4 Engineering Drive 4, Singapore* 117576)

Abstract: The $MnCO_3$ with different structures was synthesized at room temperature or by hydrothermal method. The $MnCO_3$ phase obtained at room temperature could be transferred to Mn_2O_3 plates by heat treatment at 600 ℃. In contrast, porous Mn_2O_3 nanostructures can be obtained after the heat treatment of $MnCO_3$ precursors prepared by hydrothermal method. Interestingly, Mn_2O_3 phase can be also formed by heat treatment of the $MnCO_3$ phase obtained at room temperature(Mn-RT) at 120 ℃. The products were characterized by means of XRD, SEM. The results clearly demonstrate a structure evolution from $MnCO_3$ precursors to Mn_2O_3 structures on the completion of the reaction. The formation mechanism of the above materials was further investigated by TEM and FTIR. The capacitive properties of the Mn_2O_3 materials were characterized by cyclic voltammetry. The results show that the morphologies and structures of Mn_2O_3 samples play important roles on their capacitances.

Key words: Mn_2O_3; $MnCO_3$; hydrothermal synthesis; capacitance

收稿日期:2009-11-06。收修改稿日期:2010-01-27。

国家自然科学基金(No.20803037),山东省博士基金(No.2007BS04022),山东省自然科学基金(No.ZR2009BM013)和泰山学者计划资助。

*通讯联系人。E-mail:pzguo@qdu.edu.cn;会员登记号:S060004572P。

第一作者:赵 丹,女,26 岁,硕士研究生;研究方向:微纳材料结构与性能。

Nanostructured materials for energy storage and conversation have been received more and more attention due to their potential applications in the fields of portable electronic devices and hybrid electric vehicles (HEVs)[1-3]. Supercapacitors become promising energy storage devices because of its high power density, high cycle efficiency, and long cycle life[4-5]. Precious metal oxides can show ideal pseudocapacitive behaviors, however, the high cost limits their practical applications[6-7]. Over the past decades, manganese oxides (MnO_x) have been explored due to its low cost, variable oxidation states, excellent capacitance and cycle performances[8-12]. Various manganese oxides with controlled morphologies and structures have been successfully synthesized using different approaches including hydrothermal method[13-15], sol-gel process[16-19], electrochemical route[20-21], template synthesis[22], and solution-chemical synthesis[23-25]. For example, MnO_2 film electrode showed a capacitance as high as 1 380 $F \cdot g^{-1}$, in which MnO_2 spherical grains were fabricated by a coprecipitation method using $KMnO_4$ and $MnSO_4$ as the reagents[12]. Mn_2O_3 nanoparticles can be formed via hydrothermal processes of aqueous $KMnO_4$ solutions with the addition of different alcohols[25], while Mn_2O_3 nanowires with excellent electrocatalytic properties for the reduction of O_2 can be synthesized controllably based on the systems containing $Mn(NO_3)_2$ and sodium dodecylbenzenesulfonate (SDBS)[15]. Our recent results show that organized mesoporous carbon decorated with Mn_2O_3 nanoparticles can be used as the electrode materials for supercapacitor and Mn_2O_3 nanoparticles display high specific capacitances as calculated from the content of Mn_2O_3 phase in the electrode and the increase in capacitance of the composite electrode[26]. However, the relationship between the structures and capacitances of Mn_2O_3 nanomaterials still need to be further clarified.

In this paper, the morphology-controlled synthesis of Mn_2O_3 nanostructures as well as their effect on the capacitance is studied. It is found that $MnCO_3$ aggregates or Mn_2O_3 nanostructures can be obtained based on the systems containing biomolecule L-cysteine and $KMnO_4$. These results are different from our earlier results that hexagonal γ-MnS nanorod crystals can be controllably fabricated after the hydrothermal processes of the mixed solutions containing manganese(Ⅱ) salts and *L*-cysteine[27]. The present experimental results reveal that hexagonal Mn_2O_3 nanoplates can be obtained after high-temperature treatments of the room-temperature products (Mn-RT) prepared from the reaction of $KMnO_4$ and *L*-cysteine. However, porous Mn_2O_3 nanostructures are formed after heat treatments of $MnCO_3$ precursors synthesized by hydrothermal treatments of Mn-RT samples. The electrochemical properties of these Mn_2O_3 nanostructures are studied by cyclic voltammetry.

1 Experimental

1.1 Materials

Alcohols, $KMnO_4$, Na_2SO_4 and *L*-cysteine were of analytical grade (Sinopharm Chemical Reagent Company) and used without further purification. Acetylene carbon black (99.99%) and polytetrafluorothylene latex (PTFE, 60%) were purchased form Strem Chemicals and Sigma-Aldrich, respectively.

1.2 Synthesis of Mn_2O_3 nanoplates and porous nanostructures

In a typical synthesis, aqueous $KMnO_4$ (0.474 g) solution (15 mL) was dropped into aqueous *L*-cysteine (0.363 g) solution (15 mL) under stirring. After 5 min stirring, the solution was transferred to a 40 mL teflon-lined autoclave. Hydrothermal synthesis was carried out in an oven at 120 or 150 ℃ for 24 h. The solid was collected and washed with distilled water and absolute ethanol thoroughly, and then dried in an oven at 60 ℃ for 6 h. The products obtained at room temperature, 120 and 150 ℃ are abbreviated as Mn-RT, $MnCO_3$-120 and $MnCO_3$-150, respectively. These three products were further calcined in a tube furnace at 600 ℃ in air for 3 h to obtain the as-prepared products Mn_2O_3-RT, Mn_2O_3-120 and Mn_2O_3-150, respectively. Furthermore, Mn_2O_3-RT-L sample is referred to the product of Mn-RT sample after heat treatment at 120 ℃ in air for 3 h.

1.3 Characterization

XRD patterns were recorded on a Bruker D8 Advance X-ray diffractometer equipped with graphite

monochromatized Cu Kα radiation (λ =0.154 18 nm) from 10° to 80°(2θ) using a solid detector. SEM images were taken with a JSM-6390LV scanning electron microscope operated at 20 kV. TEM images were obtained with a JEM-2000EX transmission electron microscope operated at 160 kV. FTIR spectra were measured on a Nicolet5700 FTIR spectrometer. Electrochemical measurements were performed on a CHI760C electrochemical workstation using a three-electrode cell, platinum wire as the counter electrode and saturated calomel electrode as the reference electrode in 1 mol·L^{-1} Na_2SO_4 solution, the working electrode was prepared by mixing the Mn_2O_3 samples with polytetrafluoroethylene (PTFE) and acetylene carbon black in a mass ratio of 80:15:5 and was blended to achieve a homogeneous mixture. The resulting slurry was then pressed onto a nickel foam grid(1×1 cm^2) at 15 MPa. The typical mass load of each electrode material is about 5 mg. Before measurements, the working electrodes are dipped into aqueous 1 mol·L^{-1} Na_2SO_4 solutions overnight. All potentials are reported against the saturated calomel reference electrode.

2 Results and discussion

Fig.1 shows the XRD patterns of as-prepared samples. It can be seen from Fig.1a that no crystalline phase is formed in Mn-RT sample, indicating an amorphous structure. After a hydrothermal process at 120 ℃, the XRD pattern of $MnCO_3$-120 in Fig.1b can be indexed to rhodochrosite $MnCO_3$ phase(PDF No. 86-0172). When the synthesis temperature is up to 150 ℃, the diffraction peaks in Fig.1c of sample $MnCO_3$-150 can also be well-indexed to the same $MnCO_3$ phase, and the peak at 34.4° ascribed to the(006) peak is strongly strengthened. Furthermore, the narrow and intensive diffraction peaks in Fig.1c indicate that the $MnCO_3$-150 products are well crystallized.

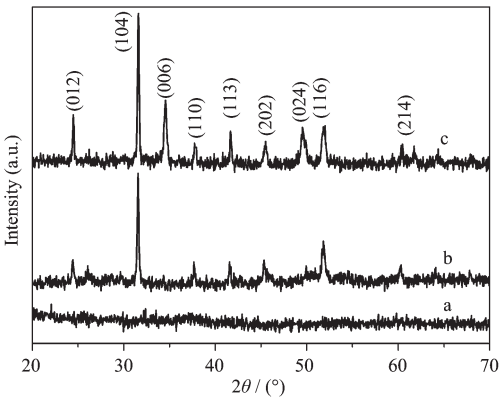

(a) Mn-RT; (b) $MnCO_3$-120; (c) $MnCO_3$-150

Fig.1 XRD patterns of the as-prepared products

The SEM images of these products are shown in Fig.2. Mn-RT (Fig.2a) shows clew-like microstructures composed of nanoparticles and some crossed wire-like structures with several micrometers long and diameter scales of tens of nanometers. It can be seen from Fig.2b that sample $MnCO_3$-120 displays spindle-like shape with length scale about 1.5~2 μm composed of $MnCO_3$ nanoparticles. However, $MnCO_3$-150 showed larger micro-aggregate structure composed of $MnCO_3$ nanoparticles compared to those of $MnCO_3$-120 (in Fig.2c). It can be observed that the reaction temperature has a strong effect on the morphology of the $MnCO_3$ products. The formation of $MnCO_3$ micro-aggregates composed of $MnCO_3$ particles could be ascribed to the Ostwald ripening that large particles grow at the expense of smaller ones[28-29]. This has been further confirmed by the results of the intermediate products synthesized hydrothermally at different reaction times. It can be observed from Fig.3a and d that both the products obtained after 2 h reaction at 120 and 150 ℃, respectively, display similar morphology to that of Mn-RT(in Fig.2a). With the reaction time extended to 4 h, however, the morphology changes dramatically (Fig.3b

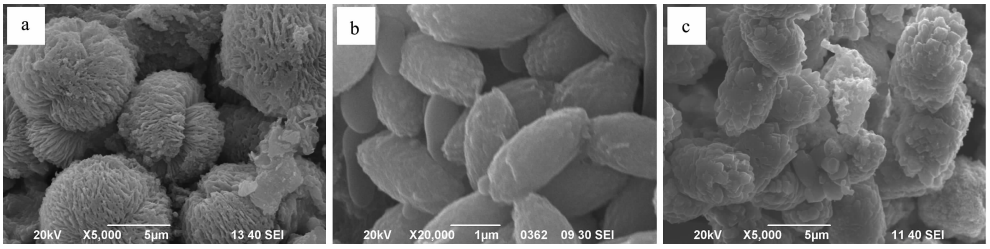

Fig.2 SEM images of Mn-RT (a), $MnCO_3$-120 (b) and $MnCO_3$-150 (c)

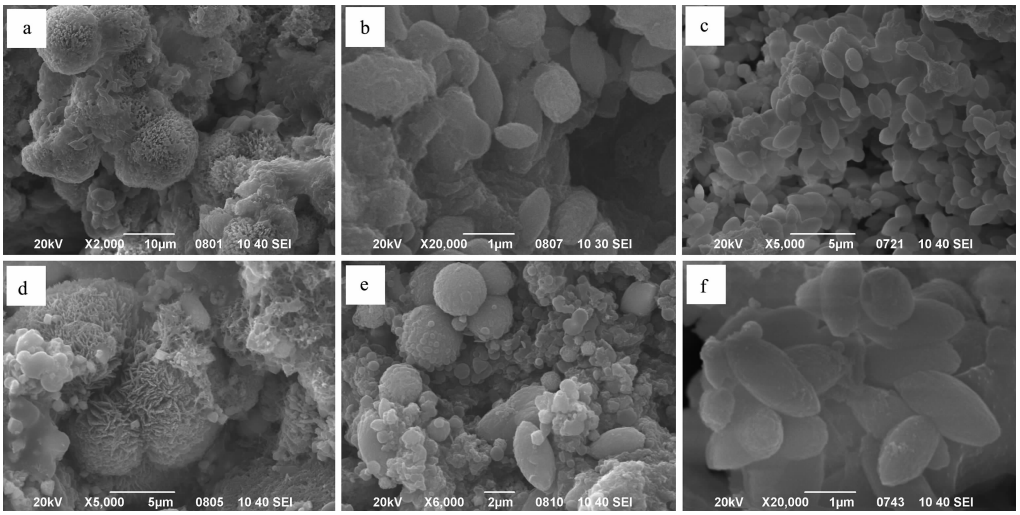

Fig.3　SEM images of the intermediate products synthesized from the mixed systems at 120 ℃ (a, b, c) and 150 ℃ (d, e, f) for 2 h (a, d), 4 h (b, e) and 8 h (c, f)

and e). When the reaction time is 8 h, spindle-like aggregates with the size less than 1 m can be observed for the products collected at 120 ℃ while somewhat larger particles and aggregates are formed when the synthesis temperature is up to 150 ℃ (Fig.3c and f).

The XRD patterns of the products obtained by different heat treatments are shown in Fig.4. It can be seen from Fig.4a ~c that the diffraction peaks in the XRD patterns of sample Mn_2O_3-RT, Mn_2O_3-120 and Mn_2O_3-150, respectively, can be well indexed to the same bixbyite Mn_2O_3 phase (PDF No. 41-1442). These results indicate that both amorphous Mn-RT sample and crystalline $MnCO_3$ products can be transited to Mn_2O_3 phases after the heat treatment at 600 ℃ in air. Interestingly, it is Mn_2O_3 phase, not $MnCO_3$ phase or MnO_2 phase, that can also be obtained for the Mn_2O_3-RT-L sample as evidenced by the XRD pattern in Fig. 4d. This is clearly different from that of sample $MnCO_3$-120 synthesized using sample Mn-RT as the raw material via a hydrothermal process at 120 ℃ . Furthermore, the total weight loss for the formation of Mn_2O_3 sample from $MnCO_3$ precursor under high temperature treatments is 31%, in good agreement with the theoretical value calculated from the following reaction:

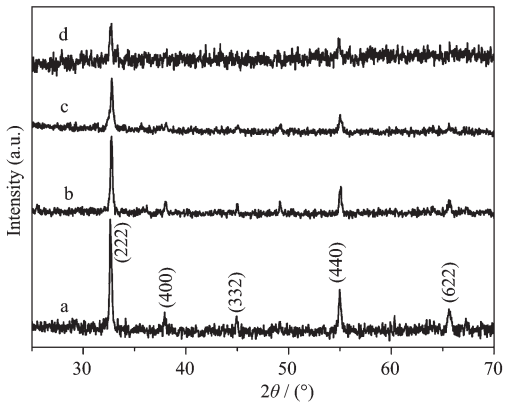

(a) Mn_2O_3-RT, (b) Mn_2O_3-120, (c) Mn_2O_3-150 and (d) Mn_2O_3-RT-L

Fig.4 XRD patterns of the calcined samples

$$4MnCO_3 + O_2 = 2Mn_2O_3 + 4CO_2 \quad (1)$$

Generally, Mn_2O_3 phases are formed from Mn-containing compounds after high temperature treatments. Recently, it is reported that Mn_2O_3 phases can be formed during the reaction of $KMnO_4$ with active mesoporous carbon materials[26] or specific alcohols[25] at room temperature. Our results show that Mn_2O_3 phase, not $MnCO_3$ or MnO_2 phase, can be formed from Mn-RT samples after low temperature treatment although impurities are also found in the sample according to the FTIR spectrum(Fig.5a). For example, the peaks at 2 922 and 2 850 cm^{-1} ascribed to CH_2 symmetric and asymmetric vibrations, respectively, appear, indicating that the alkyl groups still exist in the Mn_2O_3-RT-L samples. Two peaks at 3 422 and 1 630 cm^{-1} in Fig.5a can be observed, which are assigned to H_2O absorbed by KBr. The FTIR spectra of the Mn_2O_3 samples obtained after high temperature treatment of the precursors are obviously different from that of sample

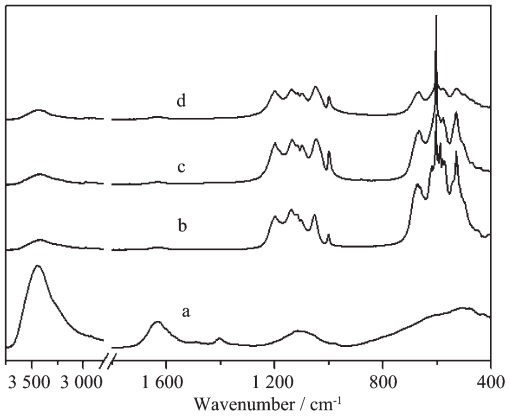

Fig.5 FTIR spectra of Mn_2O_3-RT-L (a), Mn_2O_3-RT (b), Mn_2O_3-120 (c) and Mn_2O_3-150 (d)

Mn-RT-L. From Fig.5b~d, it can be clearly seen that all the Mn_2O_3 samples show similar absorption spectra only with some differences in absorption intensities of the characteristic peaks. For example, the peaks at 3 422 and 1 630 cm^{-1} can also be observed similar to those of sample Mn-ER-L. The peaks around 530, 604, and 665 cm^{-1} and the peaks between 1 000~1 200 cm^{-1} assigned to ν_{Mn-O} of Mn_2O_3 phase [30], indicating that pure Mn_2O_3 phase can be formed after the high temperature process.

Compare to those results of the precursors shown in Fig.2, obvious change in the shape of products can be observed for the Mn_2O_3 samples. Fig.6a shows the SEM image of sample Mn_2O_3-RT-L. The sample displays irregular shapes decreasing greatly in the size of the aggregates compared with those of Mn-RT samples. This may be caused by the collapse of Mn-RT samples under heat treatments. It is interesting to note that colloidal Mn_2O_3 particles shown in Fig.6b display narrow size distribution with the size scales less than 150 nm. Spindle Mn_2O_3 microstructures with the length scales of 1~2 μm composed of colloidal particles can be observed from sample Mn_2O_3-120(Fig.6c), in which the shape and the size of the aggregates are similar to those of the $MnCO_3$-120 precursor. However, porous nanostructure aggregates can be obtained for sample Mn_2O_3-150 (Fig.6d), in which the contour of Mn_2O_3 aggregates is maintained compared with those of $MnCO_3$-150 samples. It can also be observed clearly from Fig.6d that the sizes of Mn_2O_3-150 particles are smaller than those of Mn_2O_3-120 colloidal particles.

The TEM images of Mn_2O_3 samples are shown in Fig.7. The TEM image (Fig.7a) of sample Mn_2O_3-RT displays plate-like nanostructures with clear edges and somewhat irregular~hexagonal shapes. The sizes of the Mn_2O_3-RT colloid plates are of 50~120 nm in accord with those of SEM observations (Fig.6B). The selected area electron diffraction (SAED) pattern of a single Mn_2O_3 plate in the inset in Fig.7a shows that Mn_2O_3 colloidal plates are single crystalline. The TEM image of sample Mn_2O_3-120 (Fig.7b) reveals that the porous spindle microstructures are composed of irregular colloidal Mn_2O_3 particles with the sizes similar to those of Mn_2O_3-RT. The SAED patterns of a single particle, as depicted in the inset in Fig.7b, shows that Mn_2O_3 particles are single crystalline. Interestingly, sample Mn_2O_3-150 shows similar morphology with those of Mn_2O_3-120 and is composed of Mn_2O_3 nanoparticles with the size of 30~60 nm(Fig.7c). The SAED pattern in the inset in Fig.7c shows the single crystal nature of a single Mn_2O_3 nanoparticle.

Cyclic voltammograms (CV) for Mn_2O_3 samples at different scan rates are shown in Fig.8. The CV curves of the samples are rectangular profiles at low scan rates, indicating the existence of an ideal capacitive behavior important for a system to be highly reversible. The specific capacitance of Mn_2O_3-150 in Fig.8Ca is 93 $F \cdot g^{-1}$ at the scan rate of 2 $mV \cdot s^{-1}$, which is the highest in the present study. For sample Mn_2O_3-120 and Mn_2O_3-

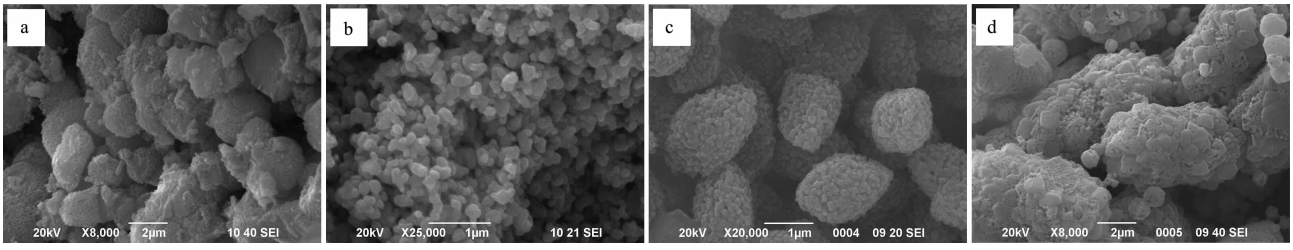

Fig.6 SEM images of Mn_2O_3-RT-L (a), Mn_2O_3-RT (b), Mn_2O_3-120 (c) and Mn_2O_3-150 (d)

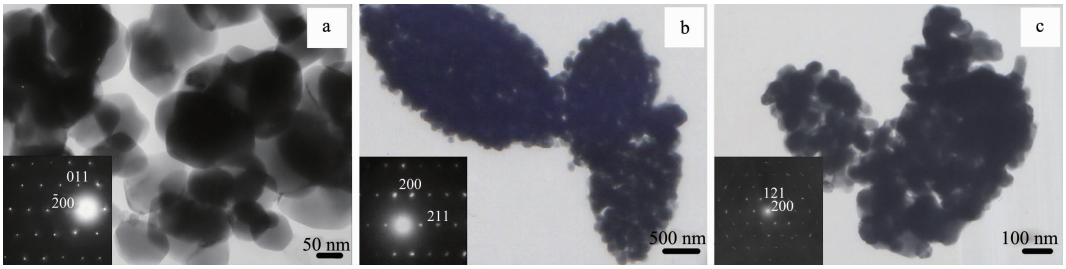

Fig.7 TEM images of Mn_2O_3-RT(a), Mn_2O_3-120 (b), and Mn_2O_3-150 (c)

RT, the specific capacitances are found to be 72 and 67 $F \cdot g^{-1}$(Fig.8Ba and Aa), respectively. If the scan rate is changed to 5 $mV \cdot s^{-1}$, the calculated specific capacitances for sample Mn_2O_3-150, Mn_2O_3-120 and Mn_2O_3-RT are 58, 50 and 51 $F \cdot g^{-1}$, respectively. The CV curves are not nearly rectangular at a scan rate of 10 $mV \cdot s^{-1}$, as shown in the c curves in Fig.8, indicating that the ohmic resistance of the samples is large at a high scan rate[31]. The main difference in the specific capacitance for these Mn_2O_3 samples may be attributed to the difference in the size and structure nature of the synthesized materials. As pseudocapacitance is related to the actual redox reactions occurring in the system, the reactivity of the samples may be strengthed by large surface area small particles with a facile diffusion of electrolyte ions. It should be pointed that the specific capacitance values of the Mn_2O_3 samples are smaller than those of MnO_2 samples[10,20]. This may be caused by the existence of the 3^+ oxidation state of Mn leading to the reduction in the specific capacitance.

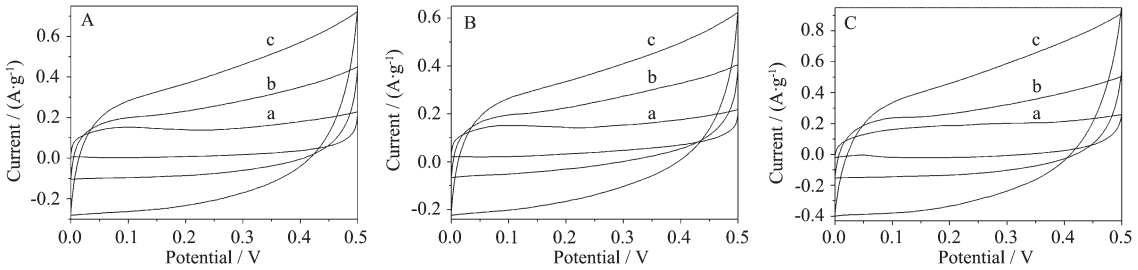

Fig.8　CV curves of sample Mn_2O_3-RT (A), Mn_2O_3-120 (B) and (C) Mn_2O_3-150 in aqueous Na_2SO_4 solutions at different scan rates of 2 $mV \cdot s^{-1}$ (a) 5 $mV \cdot s^{-1}$ (b) and 10 $mV \cdot s^{-1}$ (c)

3　Conclusions

Mn_2O_3 plates and nanoparticle aggregates were synthesized through high temperature treatment of Mn-containing precursors obtained from the mixed systems of $KMnO_4$ and *L*-cysteine. Mn_2O_3 phase could also be obtained after the heat treatment of the room-temperature products in air at 120 ℃. It is found that Mn_2O_3 colloid plates with sizes of 50 ~120 nm and Mn_2O_3 colloidal/nanoparticles are single crystalline. The specific capacitance of Mn_2O_3 samples is increased with the order of Mn_2O_3-RT, Mn_2O_3-120 and Mn_2O_3-150 at a low scan rate, where the morphology and size of the samples have strong effect on their capacitance. The formation mechanism of Mn_2O_3 nanostructures and the relationship between Mn_2O_3 nanostructures and their electrochemical properties are suggested.

References:

[1] Kötz R, Carlen M. *Electrochim. Acta*, **2000**,**45**:2483-2498

[2] Nakayama M, Tanaka A, Sato Y, et al. *Langmuir*, **2005**,**21**:5907-5913

[3] Burke A. *J. Power Sources*, **2000**,**91**:37-50

[4] Winter M, Brodd R J. *Chem. Rev*., **2004**,**104**:4245-4269

[5] Pandolfo A G, Hollenkamp A F. *J. Power Sources*, **2006**,**157**:11-27

[6] Zheng J P, Cygan P J, Jow T R. *J. Electrochem. Soc*.,**1995**, **142**:2699-2703

[7] Hu C C, Chang K H, Lin M C, et al. *Nano Lett*., **2006**,**6**:2690-2695

[8] Jiao F, Bruce P G. *Adv. Mater*., **2007**,**19**:6576-60

[9] Yu C, Zhang L, Shi J, et al. *Adv. Funct. Mater*., **2008**,**18**:1544-

1554

[10]Xu J J, Yang J. *Electrochem. Commun*., **2003**,**5**:306-311

[11]Pang S C, Anderson M A, Chapman T W. *J. Electrochem. Soc*., **2000**,**147**:444-450

[12]Toupin M, Brousse T, Belanger D. *Chem. Mater.*, **2004**,**16**: 3184-3190

[13]Du G H, Chen Q, Che R C, et al. *Appl. Phys. Lett.*, **2001**,**79**: 3702-3704

[14]Ma R , Zhang L, Sasaki T, et al. *Adv. Mater*., **2004**,**16**:918-922

[15]Cheng F Y, Shen J, Ji W Q, et al. *ACS Appl. Mater. Interfaces*, **2009**,**1**:460-466

[16]Franger S, Bach S, Farcy J, et al. *J. Power Sources*, **2002**,**109**: 262-275

[17]Lin C K, Chuang K H, Lin C Y, et al. *Surf. Coat. Technol.*, **2007**,**202**:1272-1276

[18]Chin S F, Pang S C, Anderson M A. *J. Electrochem. Soc*., **2002**,**149**:A379-A384

[19]Reddy R N, Reddy R G. *J. Power Sources*, **2003**,**124**:330-337

[20]Nakayama M, Tagashira H. *Langmuir*, **2006**,**22**:3864-3869

[21]Hu C C, Wang C C. *J. Electrochem. Soc*., **2003**,**150**:A1079-A1084

[22]Mann S. *Angew. Chem. Int. Ed*., **2000**,**39**:3392-3406

[23]Cushing B L, Kolesnichenko V L, O′Connor C J. *Chem. Rev*., **2004**,**104**:3893-3946

[24]Chandra N, Bhasin S, Sharma M, et al. *Mater. Lett*., **2007**, **61**:3728-3732

[25]Subramanian V, Zhu H W, Wei B Q. *Chem. Phys. Lett*., **2008**, **453**:242-249

[26]Zhang L L , Wei T X , Zhao X S, et al. *Micropor. Mesopo. Mater.*, **2009**,**123**:260-267

[27]GUO Pei-Zhi(郭培志), LI Hong-Liang(李洪亮), YU Jian-Qiang(于建强), et al. *Chinese J. Inorg. Chem.*(*Wuji Huaxue Xuebao*), **2008**,**24**(9):1387-1392

[28]Ostwald W Z. *Phys. Chem*., **1897**,**22**:289-330

[29]Ostwald W Z. *Phys. Chem.*, **1900**,**34**:495-503

[30]Gillot B, Guendouzi M El, Laarj M. *Mater. Chem. Phys.*, **2001**,**70**:54-60

[31]Zheng J P. *J. Electrochem. Soc*., **2003**,**150**:A484-A492